Energy & Environmental Sustainability 1 (2025) 100055

Contents lists available at ScienceDirect

Energy & Environmental Sustainability

journal homepage: www.sciencedirect.com/journal/energy-and-environmental-sustainability

Synthesis and sustainable application of fluorosilicon-based superhydrophobic coatings for high-salt wastewater treatment: A short two-step method

Zhigen Wu[a,b,*], Zihan Yan[a,c], Chenzhen Ji[d], Dan Zhou[e], Mohammad Harris[f], Hongwei Wu[f]

[a] State Key Laboratory of Water Pollution Control and Green Resource Recycling, College of Environmental Science and Engineering, Tongji University, 200092, China
[b] Shanghai Institute of Pollution Control and Ecological Security, 200092, China
[c] Shanghai Ocean Shipping Co. Ltd, 20082, China
[d] School of Mechanical Engineering, Tongji University, Shanghai, 201804, China
[e] School of Transportation and Vehicle Engineering, Shandong University of Technology, 255000, China
[f] School of Physics, Engineering and Computer Science, University of Hertfordshire, Hatfield, AL10 9AB, UK, United Kingdom

ARTICLE INFO

Keywords:
Antifouling
Coating modification
Superhydrophobic coating
High-salt wastewater
Circular economy

ABSTRACT

A fluorosilicon-based superhydrophobic coating (ER-SiO_2/PVDF/SFT) was engineered by a novel non-hydrolytic two-step methodology, demonstrating exceptional fouling resistance in hypersaline wastewater treatment. The coating achieved a water contact angle of 154.3 ± 0.5°, representing a 12 % increase over epoxy resin (ER) reference coatings – and effectively repelled organic contaminants (ethylene glycol contact angle: 148.8 ± 1.8°). Antifouling efficiency reached 70 % against $CaCO_3$ fouling deposits in simulated two kinds of high-salt fouling solution, attributable to ultralow surface energy and biomimetic hierarchical roughness. Long-term thermal fouling tests revealed <5 % hydrophobicity decay, which would save energy in thermal evaporation. The short two-step method not only prevents fouling with minimal operational complexity but also facilitates easy reapplication, reducing material waste and chemical usage while supporting a circular economy in industrial water reuse. This scalable, low-waste coating supports Zero Liquid Discharge (ZLD) initiatives and UN Sustainable Development Goals 6 and 12, making it ideal for industrial applications and sustainable resource consumption.

Nomenclature:

Abbreviation	Full Form
AR	Analytical Reagent Grade
CA	Contact Angle
PVDF	Polyvinylidene Fluoride
RG	Reagent Grade
SDG	Sustainable Development Goals
SFT	1H,1H,2H,2H-perfluorodecyltrimethoxysilane
TDS	Total Dissolved Solids
WCA	Water Contact Angle
ZLD	Zero Liquid Discharge

1. Introduction

As industrial processes undergo rapid technological evolution, the effective management of hypersaline wastewater has emerged as a paramount environmental challenge [1,2]. This wastewater stream is characterized by complex chemistry and poor biodegradability [3], with total dissolved solids (TDS) often exceeding 3.5 wt%, posing substantial obstacles to conventional biological treatment methodologies. Membrane distillation [4] and thermal evaporation [5] are commonly employed treatment methods. Evaporation has significant potential for reducing global energy consumption and environmental impact [6]. The adoption of Zero Liquid Discharge (ZLD) policies has driven the integration of these processes. Typically, the traditional membrane distillation process is preceded by thermal evaporation before concentration and crystallization [7,8]. While this integration enhances the overall treatment efficacy and ensure compliance with stringent environmental regulations. However, the associated energy-intensive consumption still remains a concern [9]. Similar to process enhancements in thermal systems—such as the use of vibrators to improve solar still efficiency [10], the superhydrophobic coating also has advantages to improve the energy efficiency of thermal evaporation.

* Corresponding author. State Key Laboratory of Water Pollution Control and Green Resource Recycling, College of Environmental Science and Engineering, Tongji University, 200092, China.
E-mail address: wuzhigen@tongji.edu.cn (Z. Wu).

https://doi.org/10.1016/j.eesus.2025.100055
Received 28 July 2025; Received in revised form 6 September 2025; Accepted 23 September 2025
Available online 23 October 2025

The energy-intensive nature principally stems from scaling deposits formed during hypersaline wastewater desalination [11]. These deposits accumulate on heat exchanger surfaces, diminishing thermal-hydraulic performance through increased fouling thermal resistance (R_f) [12] and fluid flow resistance [13,14], leading to substantial energy penalties. Consequently, mitigating heat exchanger fouling is essential for improving the economics of high-salinity wastewater desalination [15]. Research into fouling mechanisms, including computational fluid dynamics (CFD) modelling and experimental studies, has elucidated scaling nucleation and growth in high-salt environments [16,17]. A promising method involves applying protective coatings to reduce deposit adhesion without damaging surfaces [18,19]. This approach helps to maintain long-term heat transfer performance and offering a viable fouling prevention strategy for heat exchangers [20].

The water contact angle (WCA) serves as a critical hydrophobicity indicator for coating performance evaluation, with higher values ($\theta_{WCA} > 150°$) defining the superhydrophobic regime. Superhydrophobic surfaces fundamentally mitigate scaling through interfacial energy barriers, with the Cassie-Baxter state playing a pivotal role in hypersaline environments [21–23]. Micro-nano hierarchical architectures (Cassie state) trap continuous air films, reducing solid-liquid contact area compared to Wenzel wetting [24]. For this reason, the coating becomes less susceptible to infiltration and erosion, and the likelihood of contaminants also decreases.

Superhydrophobic coating technology, as a cutting-edge technology with scalability and economic feasibility, is currently playing a significant role in numerous fields. Beyond its traditional applications in oil-water separation [25–27], membrane distillation [28,29], steel anti-corrosion [30,31], superhydrophobic coatings represent a technology with transformative potential for cross-domain innovation. Moawad et al. [32] synthesized an environmentally friendly antifouling coating through a green route, where nano-copper oxide was produced. Field trials on actual ships demonstrated that the coating effectively inhibited biofouling, potentially reducing vessel maintenance costs by approximately 30 % and minimizing the impact of heavy metals on nearshore ecosystems. Zhao et al. [33] constructed a dual-layer PTFE composite coating via a synergistic anodization-spraying technique. This coating exhibits integrated functionalities of superhydrophobicity, corrosion resistance, and energy harvesting, offering an innovative solution for multifunctional protection and renewable energy collection in harsh environments. Qian et al. [34] designed a three-layer structured C/PDMS/PolyF composite coating capable of achieving zero-energy-consumption deicing by harnessing solar energy, thereby providing a long-term protective strategy for industrial materials.Consequently, durable superhydrophobic coatings present a transformative alternative by improving equipment longevity and optimising efficiency [35]. This coating technology reduces the frequency of equipment replacement, lowering material demand and waste generation. Additionally, the ease of re-synthesis and reapplication ensures low-waste maintenance, making it a sustainable option. This aligns with circular economy principles by promoting extended product lifecycles and minimizing industrial waste.

Achieving robust superhydrophobicity requires stable, reliable rough structures on metal substrates [36]. A common synthesis strategy involves doping conventional coatings with nanoparticles [37], which can help improve heat storage [38]. However, the inherent poor durability and mechanical properties of nanoparticles limit their practical application. Coatings for thermal evaporation processes in high-salinity wastewater must therefore exhibit excellent organic and salt resistance. Incorporating low surface energy substances, such as fluorosilanes, enhances hydrophobicity against both aqueous and organic media (e.g., ethylene glycol). Fluorosilanes can form molecular films with very low surface energy on any surface, which can effectively protect nanoparticles from corroding [39]. The co-preparation of composite superhydrophobic coatings by blending nanoparticles with crosslinked fluorosilanes is an efficient and straightforward method [40].

A comparative analysis of prevalent surface modification methods is summarised in Table 1. Compared with other methods, the dipping method is good at achieving defect-free fluorosilane layers on pre-roughened substrates. It leverages molecular self-assembly mechanisms whose efficacy correlates with initial substrate roughness, demonstrating stronger coating adhesion than other methods in high-salt environments. Evidently, the single operation method falls short in superhydrophobic coating modifications on stable metal heat exchanger surfaces. The cyclical thermohydraulic stresses and particulate-laden fluid erosion in high-salt evaporation systems induce progressive coating delamination, fundamentally limiting industrial implementation. This requires the superhydrophobic coatings to have a tight bond with the metal substrate. The integration of chemical etching and dipping helps to improve the adhesion of the coating to the metal substrate surface. Firm modification of superhydrophobic coatings on metal substrate surfaces can be achieved by a two-step method of ‘etching + dipping’, which makes the superhydrophobic coatings more durable and resilient. The practical advantages of these methods—low equipment demands and mild reaction conditions—make them highly suitable for industrial mass production. In contrast to conventional methods that often rely on toxic substance release or complex manufacturing, our two-step 'etching-dipping' method offers a scalable and resource-efficient alternative. This aligns with emerging trends in environmentally benign material innovations for pollution control [41].

In this work, a robust superhydrophobic coating was developed through an innovative two-step 'etching and dipping' methodology. Firstly, the nano-film was etched on the metal substrate, and secondly, the superhydrophobic coating with low surface energy was modified by a dipping method. Compared to previous studies, our coating exhibited

Table 1
The applicability of coating modification methods.

Methods		Advantages	Disadvantages
Etching	**Laser etching** [42,43]	• Good coating quality • Good surface wear resistance	• High cost • Long process time • High demand for equipment
	Chemical etching [44]	• Low cost • Controllable preparation process • Good surface wear resistance • Superhydrophobic surface with acid and alkali resistance	• Corrosive etching solutions
Deposition	**Chemical deposition** [45,46]	• Superhydrophobic surface with acid and alkali resistance	• Poor surface wear resistance • Corrosive etching solutions
	Electrochemical deposition [47]	• Precisely obtain a super hydrophobic coating	• Poor surface wear resistance • High demand for equipment
Spraying [48,49]		• Short process time	• An interface stability problem • Uneven coating thickness
Dipping [50,51]		• Low cost • Small coating loss • Low demand for equipment	• Need rough substrate base

strong adhesion to the metal substrate, with no detachment observed after several days in a high-salt environment. Moreover, this superhydrophobic coating prepared in this study demonstrated a good anti-fouling effect on high-salt wastewater containing viscous organic matters and effectively suppresses Ca^{2+} adsorption. The anti-fouling properties of the developed superhydrophobic coating were evaluated with two configured high-salt solutions. The findings revealed that the special structure on the superhydrophobic coating prevented fouling deposition in high-salt wastewater on the metal surface. Furthermore, this study aimed to contribute to environmentally responsible wastewater treatment solutions aligning with global sustainable resource management efforts. By addressing the challenges of coating durability, antifouling, and reusability, it supports the transition towards low-maintenance, long-lasting antifouling solutions that reduce operational costs and environmental impact.

2. Materials and methods

2.1. Preparation principle

The superhydrophobic metal substrate designed in this study aims to improve two major problems of traditional anti-fouling coatings. Firstly, the scale inhibition of the coating would fail easily in high-salt wastewater. And secondly, the adhesion between the coating and substrate was too weak.

First of all, the superhydrophobic modification of the coating can effectively improve the anti-fouling performance of the coating. The nanostructure provides fewer nucleation sites, which caused calcium carbonate to change from calcite to aragonite. As shown in Fig. 1, the prepared superhydrophobic surface can make the water droplets and glycol droplets roll freely, and carry away floating deposits to the greatest extent during the rolling process of the droplets.

Secondly, the two-step method of etching and dipping enhanced the adhesion of the coating to the metal substrate. In the common spray preparation process, as shown in Fig. S1 (a), the natural adhesion of the coating to the smooth substrate was weak, and the coating easily detached. In the chemical deposition method, as shown in Fig. S1 (b), the coating solution was naturally deposited on the substrate by gravity. The formed superhydrophobic film was fragile because the wear resistance of nanoparticles was poor. In this study, as shown in Fig. S1 (c), the surface roughness of the substrate was increased by etching to improve the adhesion of the coating to the etched substrate, and the nanoparticles was firmly adhered to the surface of the metal substrate through the epoxy resin. Through repeated immersion, lifting and evaporation of the coating, the connection between the superhydrophobic coating and the substrate was tight and firm.

2.2. Material preparation

Pure aluminium sheets (≥99.6 % purity) were sourced from Guangzhou Xinhong New Material Technology Co. Ltd. Hexamethylenetetramine ($C_6H_{12}N_4$, 0.1 mol/L) and zinc nitrate ($Zn(NO_3)_2$, 0.1 mol/L) standard solutions were purchased from Shenzhen Bolinda Technology Co., Ltd and Shandong Metallurgical Science Research Institute Co., Ltd, respectively. Epoxy resin (E51) and curing agent (T31) were obtained from Qingdao Yusuo Chemical Technology Co., Ltd.

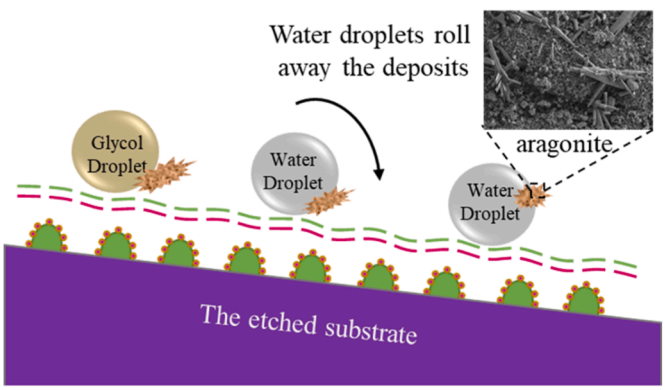

Fig. 1. Schematic diagram of superhydrophobic coating anti-fouling efficiency.

The hydrophobic powder—silicon dioxide (SiO_2, 20 nm, 99.0 %) and polyvinylidene fluoride (PVDF, RG, Mw 1,000,000)—was supplied by Shanghai Titan Scientific Co., Ltd, which also provided sodium sulfate (AR, ≥99.0 %) and other reagents: isopropyl alcohol (AR, ≥99.7 %), ethylene glycol (AR, ≥99.5 %), anhydrous ethanol (AR, ≥99.7 %), 1H,1H,2H,2H-perfluorodecyltrimethoxysilane (SFT, RG, >97.0 %), anhydrous calcium chloride (AR, >96.0 %), sodium bicarbonate (AR, ≥99.5 %), and anhydrous magnesium chloride (AR, 99.0 %). Hydrochloric acid (3 %) was used for substrate pre-treatment.

2.3. Preparation of superhydrophobic surfaces

The aluminium sheet (20 × 20 mm, used as a preparation base for hydrophobic coatings) was repeatedly sanded for 20 min and then immersed in anhydrous ethanol ultrasonic for 10 min to remove the surface oil and metal powder. After that, it was cleaned with deionized water and then dried in the oven at 60 °C for 1 h. Then, the aluminium sheet was immersed in 1 % hydrochloric acid for 5 min. After small bubbles appeared on the surface, it was repeatedly cleaned with deionized water and dried in a vacuum drying oven at 60 °C for 1 h. In order to let the superhydrophobic coating have better adhesion on the smooth metal surface, the short two-step method was used to prepare the superhydrophobic aluminium sheets, and the specific preparation process was shown in Fig. 2.

(1) First step: Surface etching

Equal amounts of hexamethylenetetramine solution ($C_6H_{12}N_4$, HMTA, 0.1 mol/L) and zinc nitrate solution ($Zn(NO_3)_2$, 0.1 mol/L) were taken separately. HMTA solution was slowly added dropwise into the Zn $(NO_3)_2$ solution. After sealing, the solution was continuously stirred for 20 min to obtain the mixed homogeneity of the clarified etching solution. The pretreated pure aluminium sheet was placed vertically in the above-prepared etching solution, sealed and placed in a 95 °C constant temperature water bath for 1 h until the reaction was complete. The etched pure aluminium was taken out, rinsed repeatedly with deionized water, and dried in an oven at 60 °C to obtain the etched aluminium sheet.

(2) Second step: Coating modification

The ER solution and curing agent solution were dissolved in isopropanol solution at the ratio of 4:1, followed by ultrasonic dispersion for 1 h to obtain a 1.43 g/L isopropanol solution of ER and a 0.36 g/L isopropanol solution of the curing agent. The mixture was then stirred continuously with a magnetic stirrer to form a well-mixed suspension.

(a) ER coating: The isopropanol solution of the ER was mixed with the isopropanol solution of the curing agent, and the mixture was ultrasonic treated at a temperature below 20 °C. Then the ER coating solution was obtained.
(b) ER-SiO_2 coating: The isopropanol solution of the ER, to which 0.7 % nano-SiO_2 was added, was mixed with the isopropanol solution of the curing agent, and the mixture was ultrasonic-treated at a temperature below 20 °C. Then the ER-SiO_2 coating solution was obtained.
(c) ER-SiO_2/PVDF/SFT coating: The isopropanol solution of the ER was supplemented with 0.7 % nano-SiO_2, 0.4 %–1.7 % PVDF, and 3.0 % of SFT. Then mix the isopropanol solution with curing agent, and the mixture was ultrasonic-treated at a temperature

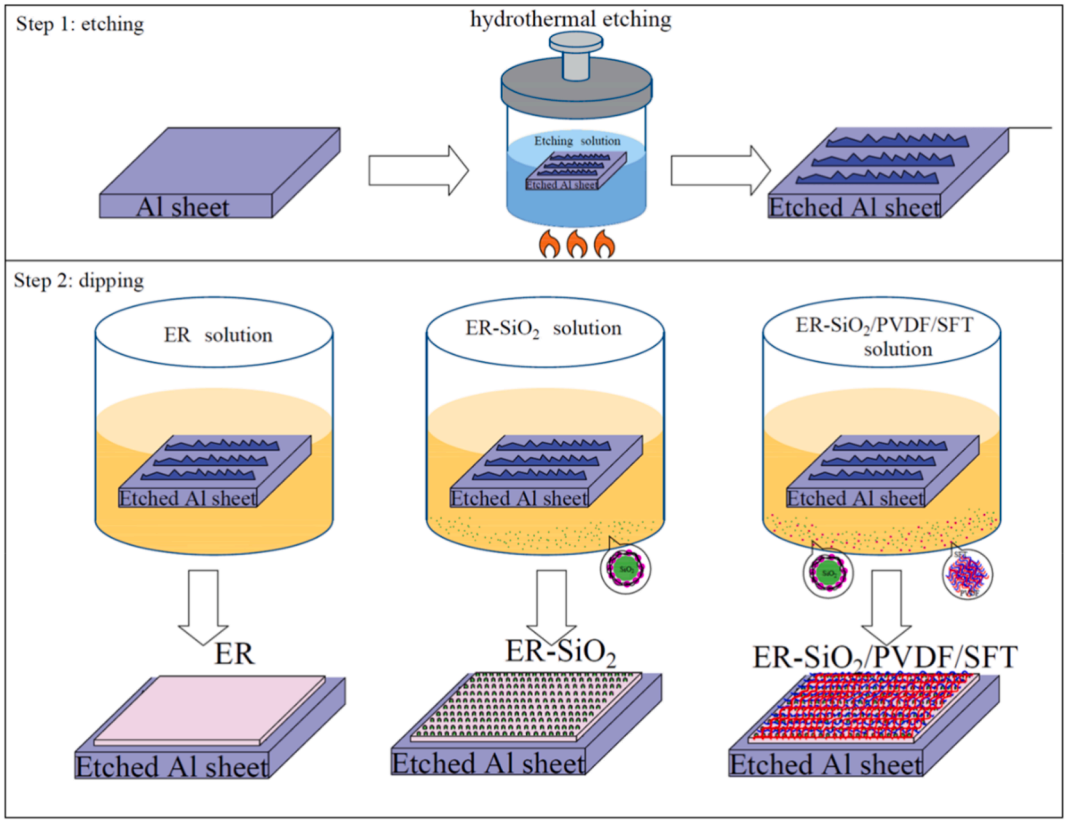

Fig. 2. Schematic diagram of the superhydrophobic coating modification.

below 20 °C. As a result, the ER-SiO_2/PVDF/SFT coating solution was obtained.

The etched aluminium sheets were soaked in different coating solutions (ER, ER-SiO_2 and ER-SiO_2/PVDF/SFT coating) for 20 min, and then dried at room temperature for 20 min. All the above steps were repeated three times to reinforce the coating thickness. The samples were all baked in a 180 °C oven for 1 h until the coating was fully cured. The prepared superhydrophobic surface thickness was about 3~5 μm. At this point, the aluminium sheet modified with the superhydrophobic coating was prepared.

2.4. Preparation of fouling test

(1) Preparation of fouling solution.

Common types of fouling deposits in heat exchangers include carbonate scales such as $CaCO_3$ and $MgCO_3$ [52]. In this experiment, a mixed solution of $CaCl_2$/$MgCl_2$ and $NaHCO_3$ was used to adjust the fouling rate by controlling the reaction temperature. Using $CaCl_2$, $MgCl_2$ and $NaHCO_3$ as raw materials, the reaction fouling solution was prepared according to the molar ratio of 1:1:2. The following reaction equations may be involved:

$$CaCl_2+2NaHCO_3 \rightarrow CaCO_3\downarrow+2NaCl + H_2O + CO_2\uparrow$$

$$MgCl_2+2NaHCO_3 \rightarrow MgCO_3\downarrow+2NaCl + H_2O + CO_2\uparrow$$

Among them, both $CaCO_3$ and $MgCO_3$ precipitated slowly.

Notably, wastewater in the evaporative wastewater treatment industry typically exhibits high salinity, high hardness, and elevated levels of COD, often accompanied by viscous substances. Ethylene glycol, a water-soluble waxy compound commonly found in wastewater, can easily migrate to aquatic environments [53]. To simulate complex industrial conditions, this experiment configured two types of fouling solutions. One was to use the viscosity of ethylene glycol to mimic the COD and viscous substances in the solution, and the other was to introduce sodium sulfate (Na_2SO_4) to replicate sulfate-containing chemical wastewater such as pharmaceuticals. The electrical conductivity of the fouling solution A and fouling solution B is 4.47 mS and 31.2 mS respectively, as shown in Table S1.

(2) Design and construction of fouling experiment system

As shown in Fig. 3 (a), the study of fouling deposit formation adopted the hanging sheet method. In the static fouling test, the samples were placed on the holding device. Then the holding device was immersed in a beaker containing fouling solution and placed on the heating table at 80°C. The schematic diagram of the device is shown in Fig. 3 (b). The temperature difference between the top and bottom of the fouling solution in the beaker should not exceed 1 °C. The external thermal insulation cover was installed.

In the experimental test, the anti-fouling performance of the coating was expressed by three indexes, fouling weight of deposits (1), fouling rate of deposits (2) and anti-fouling efficiency (3). The specific formulas are as follows:

$$\Delta m = m_2 - m_1 \tag{1}$$

where m_1 was the initial weight of the substrate, m_2 was the weight of the substrate after a period of fouling, Δm is the fouling weight of deposits.

$$v = \frac{\Delta m}{\Delta t} \tag{2}$$

$$\eta = \frac{m_2 - m_0}{m_0} \times 100\% \tag{3}$$

where, Δt was the fouling time, m_2 was the weight of the substrate

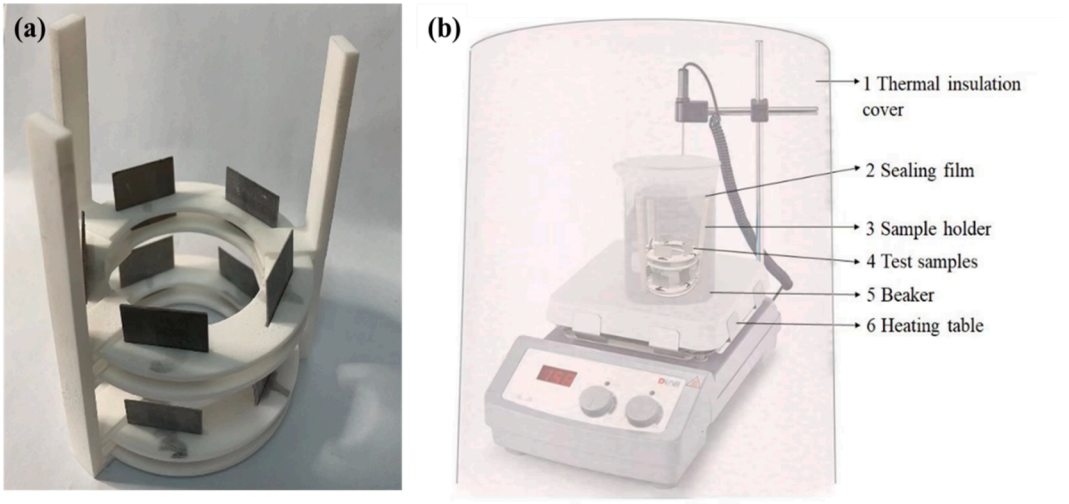

Fig. 3. (a) Sample holding device; (b) The schematic diagram of a device for fouling.

modified with coatings after a period of fouling, and m_0 was the weight of the pure metal substrate after the same period of fouling as m_2. v was the fouling rate of deposits and η was the anti-fouling efficiency. The anti-fouling efficiency compared to pure aluminium was based on the amount of fouling deposits of pure aluminium after a period of fouling.

2.5. Characterisation instruments

A contact angle instrument (JC2000d) was used to take 5 μL water droplets or glycol droplets and tested the contact angle of each sample. A total of five independent samples were prepared and tested for each coating group to confirm reproducibility. For each sample, measurements were taken at five different locations, and the average value along with the standard deviation was calculated to ensure statistical reliability.

The surface roughness of the superhydrophobic samples was characterised by atomic force microscopy (AFM, Bruker Dimension Icon). The surface morphology and size of the superhydrophobic and fouling samples were characterised by scanning electron microscopy (SEM) and energy dispersive spectroscopy (EDS) (ZEISS Gemini 300). The crystal structure of the surface of the sample was characterised by an X-ray diffractometer (XRD, Bruker D8 Advance).

3. Results and discussion

3.1. Characterization and analysis of superhydrophobic samples

3.1.1. Etching surface topography

This study focused on the anti-fouling performance of superhydrophobic coatings, and the selection of metal substrates was mainly simple and convenient. The aluminium sheets were etched to achieve an exquisite ZnO film. The aesthetic characteristics of the aluminium samples were characterised by SEM, EDS and XRD.

From the SEM characterisation depicted in Fig. 4 (b) and (c), it was observed that many rod-like and cluster-like ZnO crystals intricately grew on the surface of the underlying substrate after etching. ZnO had a length of about 10 μm and an average particle size of about 600 nm.

EDS and XRD detection and analysis were conducted on pure aluminum samples and etched aluminum samples respectively, as shown in Table S2 and Fig. 4 (a). Judging from the characterization results of EDS, after etching, the content of aluminum element on the samples decreased from 94.7 % to 3.75 %, the content of oxygen element increased from 5.3 % to 22.92 %, and a new element Zn appeared. Similarly, XRD results indicated that the characteristic peaks of ZnO appeared at 31.8° (100), 34.4° (002) and 36.3° (101) on the etched aluminum samples. Meanwhile, there were no discernible impurity peaks on the surface except ZnO and Al. The above results proved that the aluminium sheets had been etched.

3.1.2. Coating surface topography

After the etching was completed, different coatings were modified on substrates respectively. According to the SEM images, the coating surface morphology was observed. As shown in Fig. 4 (d), ZnO crystals were observed to be crystallized on the surface of ER-coated samples. From Fig. 4 (e) and (f), the agglomeration structure of silica was evident, with many small lumps on its surface resembling the micro-nano structure of a lotus leaf.

Regarding the coverage of the ER-SiO_2/PVDF/SFT coating, as shown in Fig. 4 (f), textile-like rough structural fragments were visible. The trapped air formed a buffer within the three-dimensional network structure, creating favourable conditions for achieving superhydrophobicity. Obvious holes and micro-sized protrusions formed on the surface reduced the contact surface between the droplet and the texture [54]. Robust superhydrophobicity could be realised by structuring surfaces at two different scales, with a nanostructure design to provide water repellency and a microstructure design to provide durability [55]. For example, lotus, as shown in Fig. 4 (g), multiple outward convex structures were present on the surface of the agglomeration structure, ensuring durable superhydrophobicity.

3.1.3. Fouling layer morphology

Independently designed fouling tests were conducted to test the anti-fouling ability of different coatings respectively, and the superior anti-fouling performance of superhydrophobic coatings was further analyzed. The exceptional antifouling performance can be directly correlated to the unique micro-nano structural features revealed by SEM analysis. Figs. 5 and 6 illustrated the surface topography of each substrate after being immersed in the fouling solution A and B for 7 days, respectively. The fouling solution A referred to the fouling solution containing 3 % ethylene glycol, and the fouling solution B referred to the fouling solution containing 4 % Na_2SO_4.

As shown in Fig. 5 (a)~(d), in the order of (a) pure aluminium sheet, (b) ER-coated sample, (c) ER-SiO_2-coated sample and (d) ER-SiO_2/PVDF/SFT-coated sample, the surface of the substrate became progressively less soiled. On the surface of the pure aluminium sheet and the ER-coated sample, the calcium (Ca) content in the fouling deposit substances all exceeded 25 %, and the fouling deposits were mostly $CaCO_3$ in the form of calcite. As shown in Fig. 5 (c), there was still a small amount of $CaCO_3$ in

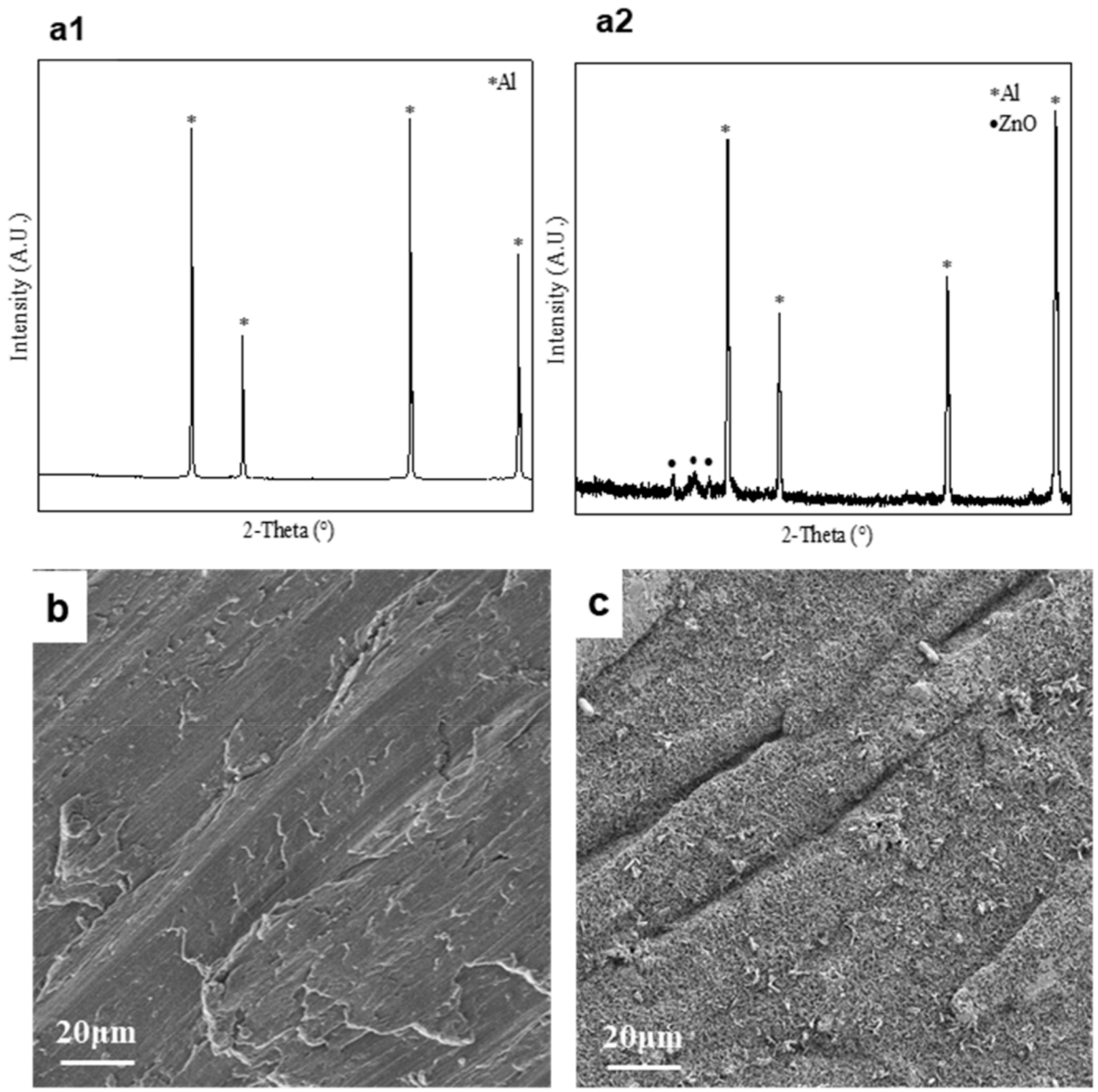

Fig. 4. Diagram of XRD images of (a1) pure and (a2) etched Al samples, and SEM images of (b) pure Al sample, (c) etched Al sample, (d) ER-coated, (e) ER-SiO_2-coated, (f) ER-SiO_2/PVDF/SFT-coated samples and (g) lotus [21].

the form of calcite on the ER-SiO_2-coated sample, but the main fouling deposits were aragonite crystals. Furthermore, as shown in Fig. 5 (d), the crystal coverage was significantly reduced, with only a few aragonite crystals present on the ER-SiO_2/PVDF/SFT-coated sample.

Based on the SEM images in Fig. 6 (a)~(c), fouling deposits were mostly hexagonal prisms. A small amount of narrowed rod-like hexagonal prism fouling deposits appeared on the ER-SiO_2/PVDF/SFT-coated sample in Fig. 6 (d). Narrower and longer fouling deposits were easier to remove through methods such as ultrasonic vibration. With the improvement of the hydrophobic performance of the coating, the fouling deposits on the surface decreased, and the Ca content dropped from 32.71 % on the pure aluminium sheet to 13.42 % on the ER-SiO_2/PVDF/SFT-coated sample.

Calcite required external forces for removal such as scraping or pickling. However, the aragonite crystals could be removed by water flushing or slight ultrasound. Compared with calcite (the most stable crystalline form of $CaCO_3$), sub-stabilised aragonite had a looser structure and higher solubility [56]. Based on the XRD images, it was evident that the superhydrophobic coating prepared in this study had good anti-fouling efficiency, as the fouling deposits were mostly loose aragonite crystals. Based on the above scale characterization analysis, it was seen that the superhydrophobic coating reduced the deposition probability of $CaCO_3$ and to a certain extent changed the size of calcium carbonate crystals, making them evolve in a direction that was easier to remove.

This minimal fouling deposition is a direct consequence of the Cassie-Baxter state. The reduced solid-liquid contact area not only enhanced hydrophobicity but also provided fewer nucleation sites for scale formation, effectively suppressing the deposition and adhesion of foulants. Further characterization of the samples after fouling of the superhydrophobic coating revealed that there were still papillary superhydrophobic structures on the sample surface. It can be seen that $CaCO_3$ grew on the peaks of the nano-papillae, as shown in Fig. S2 (a). This observation confirmed the stability of the Cassie-Baxter state even under fouling challenge. The foulants primarily nucleated on the peaks of the micro-nano structures, leaving the air-filled valleys intact and thus preserving the coating's non-wetting properties. The small contact area of the papillary peaks resulted in only a few nucleation sites on the coating surface, making it difficult for $CaCO_3$ crystals to adhere [57]. Additionally, the molecular film formed by the co-construction of SFT and PVDF was modified on the surface of nano-SiO_2, creating a thicker

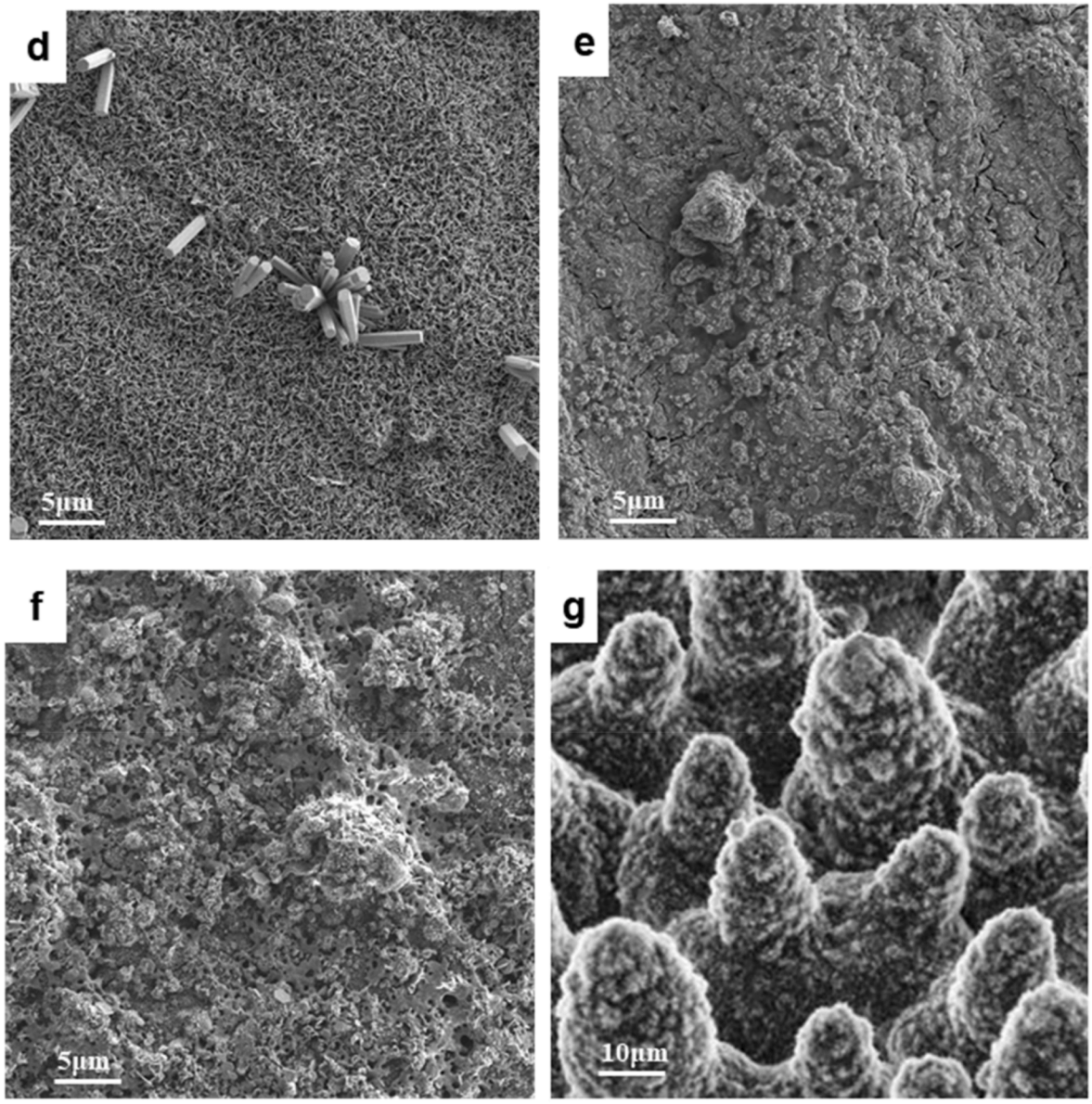

Fig. 4. (*continued*).

air film [22]. As shown in Fig. S2 (b), the air film effectively prevented the passage of salt ions and glycols, making it impossible for fouling deposits to penetrate the coating and only nucleate on the surface of the rough structure [58], thus maximizing the protection of the papillae from damage. This metastable interface suppresses ionic diffusion and disrupts crystalline nucleation, preferentially inducing weakly-adherent aragonite formation over calcite.

3.2. Analysis of superhydrophobicity of coatings

3.2.1. Contact angle

(1) Superhydrophobic performance of the ER-SiO_2/PVDF/SFT coating

Polyvinylidene Fluoride, notably known as PVDF, represents an exceptionally robust thermoplastic fluoropolymer [59,60] and is suitable for applications requiring resistance to solvents as well as acid and alkali erosion [61]. However, PVDF has a strong curing property, for which excessive addition can easily lead to delamination of the coating solution. 1H, 1H, 2H, 2H-Perfluorodecyltrimethoxysilane (hereinafter referred to as SFT) is a good modification of low surface energy modification material [62]. With the addition of SFT and PVDF substances, the WCA and ethylene glycol CA of the samples were effectively increased. As per Fig. S3 and Fig. S4, it was verified that the superhydrophobicity of the ER-SiO_2/PVDF/SFT coating was better than that of the ER and ER-SiO_2 coatings. The ER-SiO_2/PVDF/SFT coatings effectively amplified the WCA of the substrate from 137.0 ± 1.5° to 154.3 ± 0.5° and significantly increased the ethylene glycol CA of the substrate from 58.5 ± 2.7° to 148.8 ± 1.8°. This superhydrophobicity was highly reproducible across five independently prepared samples (Standard Deviation of WCA <0.7°), confirming the robustness of our two-step synthesis protocol.

In this work, 3.0 % SFT was added to the coating material, and then doped with different contents of PVDF ranging from 0.4 % to 1.7 %. Subsequent observations of changes in the CA of the coating surface were shown in Fig. 7 (a), along with the results of WCA and ethylene glycol CA evaluations. With the increase of PVDF content, the WCA increased initially and then decreased, while the ethylene glycol CA continuously ascended until it approached 150°. Specifically, when the content of

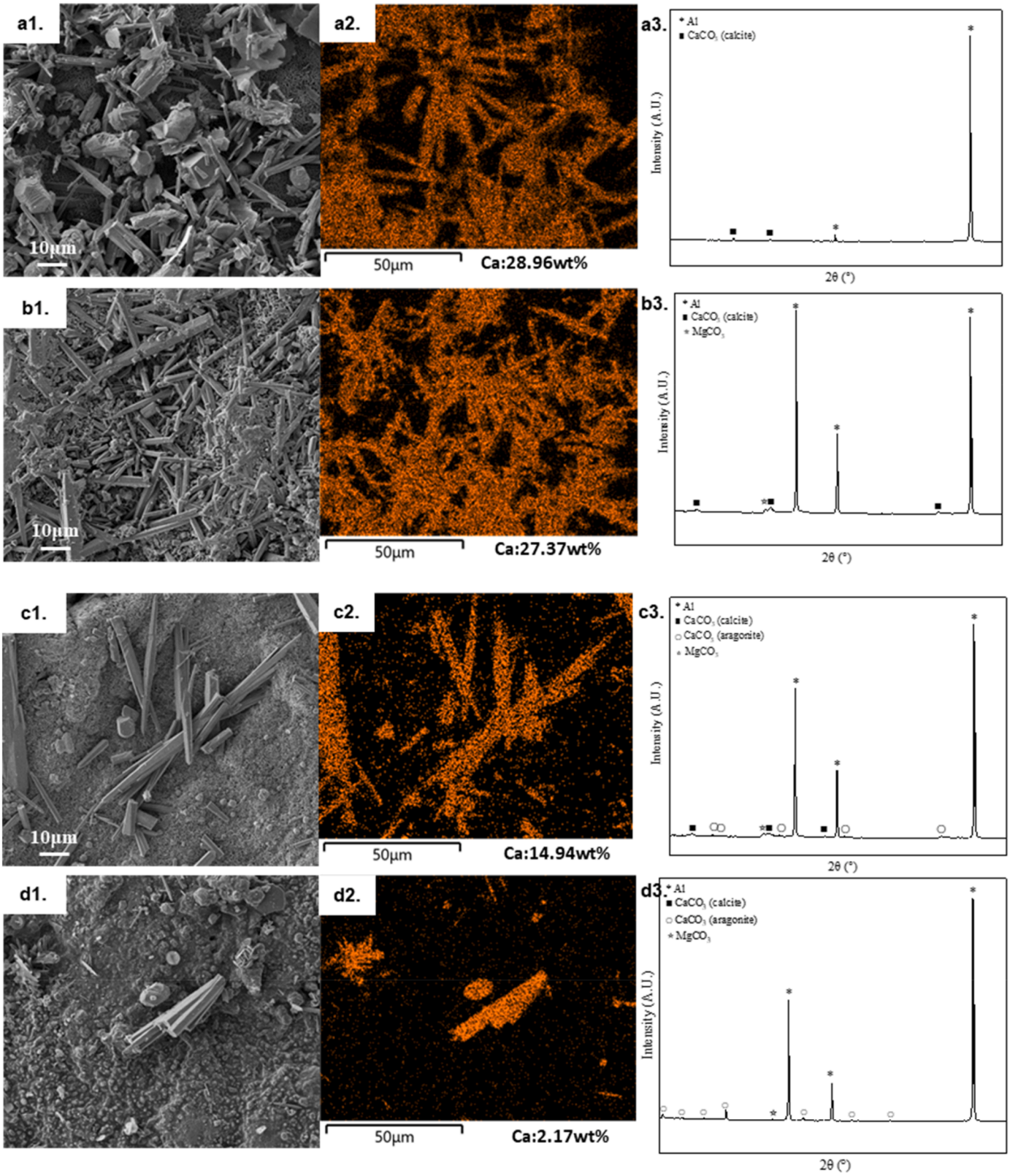

Fig. 5. Characterization images of samples after 7-day fouling in fouling solution A. (among these, (a) pure aluminium sheet, (b) ER-coated, (c) ER-SiO_2-coated and (d) ER-SiO_2/PVDF/SFT-coated samples).

PVDF was 0.7 %, the average static WCA and static ethylene glycol CA were the best. The optimal wettability at this specific composition (0.7 % PVDF) corresponded to the most stable Cassie-Baxter state, minimizing solid-liquid contact and thus maximizing the observed contact angles. The optimal performance at 0.7 % PVDF was consistent across five separate experimental batches, demonstrating the method's reliability.

The rapid curing performance of PVDF affected the WCA change of the ER-SiO_2/PVDF/SFT coating. At room temperature, accelerated

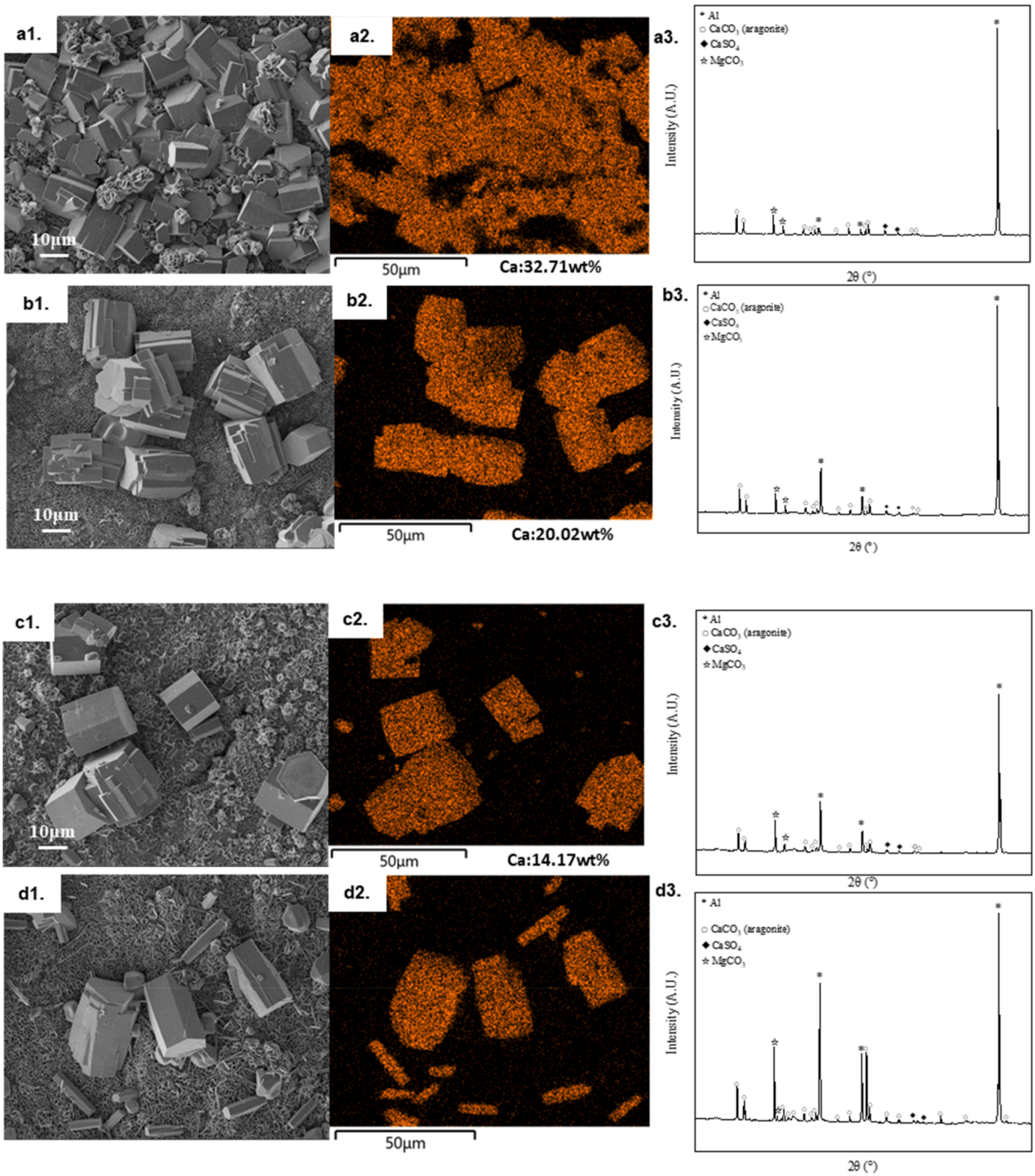

Fig. 6. Characterization images of the samples after 7-day fouling in fouling solution B. (among these, (a) pure aluminium sheet, (b) ER-coated, (c) ER-SiO_2-coated and (d) ER-SiO_2/PVDF/SFT-coated samples).

curing was observed when the PVDF content was higher than 1.0 % during testing. As shown in Fig. 7 (b), obvious delamination was seen after standing at room temperature for 12 h without adding the ER curing agent. When the curing agent was added and the mixture was left at room temperature for 6 h, the stratification phenomenon became more obvious. Curing delamination indicated that the coating solution was more difficult to preserve at room temperature for a long time. Therefore, it was determined that adding 0.7 % PVDF to the coating was optimal, and subsequent preparation tests should be conducted according to this specific proportion.

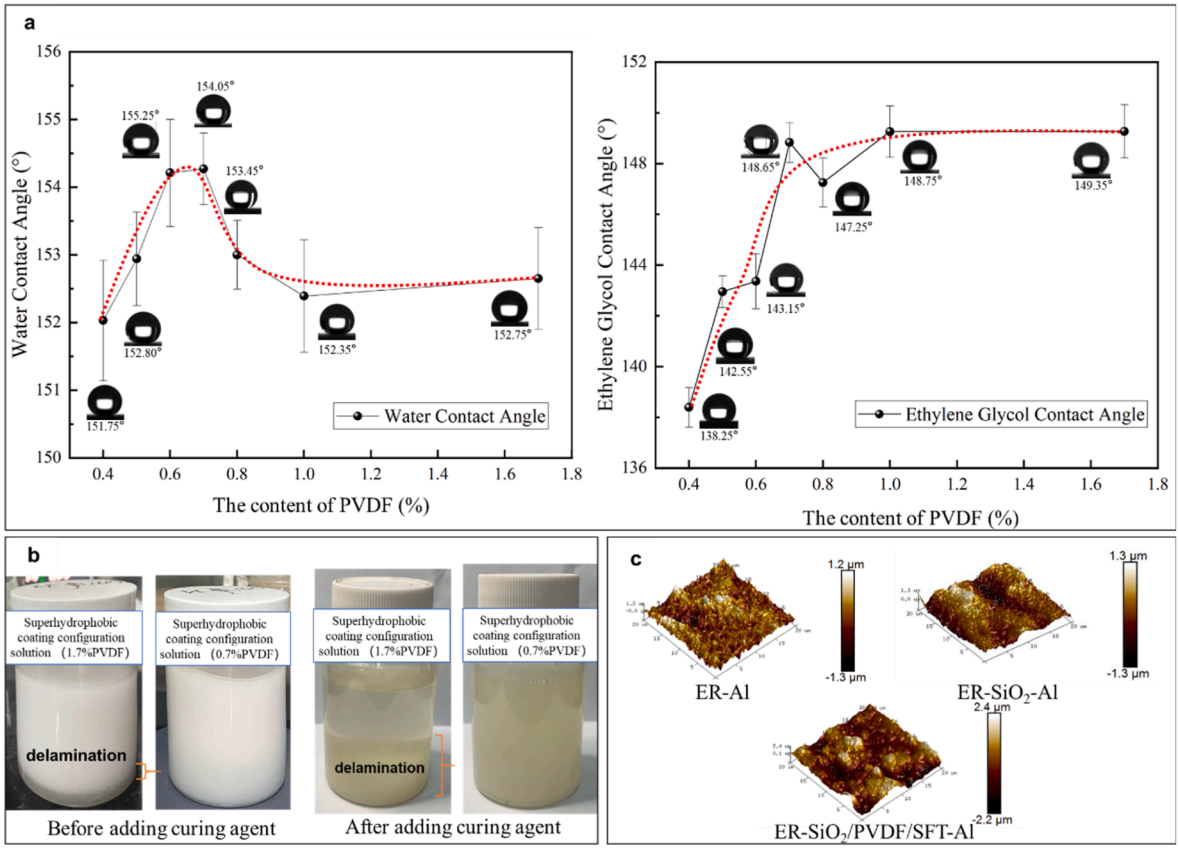

Fig. 7. Effect of PVDF content on (a)WCA and (b)Ethylene glycol CA of samples modified with ER-SiO_2/PVDF/SFT coatings.

(2) Superhydrophobic performance after 7-day fouling test

After a 7-day fouling test, the substrates modified with different coatings were carefully rinsed and repeatedly soaked with deionized water to remove loose deposits on the surface. WCA tests were performed on samples after fouling in high-salt solution A and B. The test results were presented in Table 2.

The smaller the attenuation of the WCA, the greater the durability of the coating. It was found that after a 7-day fouling challenge, the performance of the ER coatings in both high-salt solutions gradually decayed, and their surfaces exhibited a moderate degree of hydrophilicity. However, the WCA of the ER-SiO_2/PVDF/SFT-coated samples only showed a slight downward trend. In the case of ER-SiO_2/PVDF/SFT-coated samples in the fouling solution A, the WCA decreased by only 5.0 % whereas only 3.8 % in solution B, which has better durability compared to the coatings studied by previous researchers [63]. Notably, the WCA values showed low variability, underscoring the coating's consistent antifouling performance under harsh conditions.

The ER-SiO_2/PVDF/SFT superhydrophobic coating displayed remarkable resistance to permeation by concentrated salt solution, maintaining the WCA>145°, and the performance was significantly improved compared with the polymer coatings. It was verified that the ER-SiO_2/PVDF/SFT coating had excellent durability and could maintain superhydrophobicity in high-salt environment for several days.

Within broader surface engineering applications, it is noted that the pursuit of durable coatings is a critical challenge in thermal water treatment systems. The minimal performance variance of the coating across replicates are essential metrics for assessing its potential for industrial deployment.

3.2.2. Surface roughness

The AFM roughness characterisation of the superhydrophobic surface was shown in Fig. 7 (c). It was found that the roughness of the ER-coated samples was sharper, and the roughness fluctuation was small. The average roughness Ra of the surface was 246 nm, while the ER-SiO_2-coated samples and superhydrophobic ER-SiO_2/PVDF/SFT-coated samples had an obvious papillae shape with larger surface fluctuation. The measured surface roughness values were 275 nm and 545 nm for the ER-SiO_2-coated samples and ER-SiO_2/PVDF/SFT-coated samples, respectively.

The significantly increased roughness (Ra = 545 nm) of the ER-SiO_2/PVDF/SFT coating was a primary factor enabling the Cassie-Baxter state. This micro-nano hierarchical structure, analogous to the lotus leaf effect, trapped a continuous air film [22], which drastically reduced the solid-liquid contact area and was directly responsible for the high WCA (154.3 ± 0.5°) observed. The results indicated a positive correlation between surface roughness and WCA. Specifically, surfaces with larger micro-roughness were more likely to form superhydrophobic structures.

Table 2
The result of WCA on coated substrates after fouling test in solution A and B.

	ER	ER-SiO_2	ER-SiO_2/PVDF/SFT
Fouling test in solution A			
Before fouling test	137.0 ± 1.5°	149.5 ± 1.4°	154.3 ± 0.5°
Fouling for 168h	49.7 ± 0.1°	57.1 ± 0.7°	**146.5 ± 0.9°**
Attenuation ratio	63 %	62 %	5.0 %
Fouling test in solution B			
Before fouling test	137.0 ± 1.5°	149.5 ± 1.4°	154.3 ± 0.5°
Fouling for 168h	39.2 ± 0.5°	99.5 ± 0.5°	**148.5 ± 1.0°**
Attenuation ratio	71 %	33 %	3.8 %

3.3. Anti-fouling performance of coatings

3.3.1. Self-cleaning properties

The self-cleaning performances of the coatings arose from the

combination of their hydrophobicity and lower adhesion capabilities [64,65]. We tested the self-cleaning properties by dropping water droplets with a dropper, as shown in Fig. S5 and Video S2. When water droplets rolled on the surface of the pure aluminium sample, they did not wash away the sand. However, when testing ER-SiO_2/PVDF/SFT--coated samples, where water flowed through, all the sand on the coating surface was completely removed, leaving no traces of water droplets.

Regarding the adhesive effect of water drops [66], it could exhibit a remarkable capacity to absorb substantial quantities of sand. A liquid-air layer appeared on the surface of the superhydrophobic samples, which allowed the water droplets to roll, thus carrying the sand particles away and achieving self-cleaning properties [26]. This self-cleaning capability diminished the likelihood of fouling deposit accumulation and improved anti-fouling performance [67].

3.3.2. *Anti-fouling properties*

To study the effect of different salt compositions on the antifouling capabilities of the superhydrophobic coating, two types of fouling solution were used to conduct experiments. The fouling solution A referred to the fouling solution containing 3 % ethylene glycol, which represented the viscous organic matter in high-salt wastewater. And the fouling solution B referred to the fouling solution containing 4 % Na_2SO_4, representing a highly saline substance in high-salt wastewater. The fouling solution was replaced every 24 h so that the amount of fouling deposits in the solution remained relatively constant and sufficient during the 24-h test. The fouling rate would not be slowed down by the reduction of fouling deposits in the solution.

(1) Fouling observation

As shown in Fig. S6, when soaked in fouling solution, the aluminium sheets were seriously corroded by chloride ions, and the aluminium sheets began to turn black, while a large amount of white fouling deposits were attached to the substrate. At the same time, it was seen that the substrates modified with ER and ER-SiO_2 coatings began to appear some circular mottling, which was because the coatings were corroded by salt ions in the high-salt solution and started to fall off. A small amount of white fouling deposits began to appear on the surface.

In contrast, there was no obvious difference before and after fouling on the surface of aluminium sheets modified with superhydrophobic ER-SiO_2/PVDF/SFT coating, and fouling deposits were difficult to observe visually.

(2) Fouling weight

The resulting 7-day fouling curve was outlined in Fig. 8. It was seen that the fouling process was roughly divided into two stages. The first stage was the rapid fouling period (0∼24h), and the second stage was the stable fouling period (24∼168h).

The increase in substrate fouling primarily depended on the initial stage. The weight of fouling deposits was closely related to the fouling rate in the rapid fouling period. As shown in Fig. S7, the higher the rate in the rapid fouling period, the greater the weight of fouling deposits in the whole cycle (7-day fouling in this study). The fouling rate of the pure aluminium sheets in the initial 0∼24h was about four times that of 24∼168h. In contrast, the fouling rate of the superhydrophobic ER-SiO_2/PVDF/SFT-coated substrate remained nearly constant throughout the 7-day period.

Due to the fouling increment of the substrate being mainly dependent on the first stage, a longer fouling induction period indicated better coating performance. It was worth noting that only the superhydrophobic ER-SiO_2/PVDF/SFT-coated samples had a significant fouling induction period, during which minimal deposit formation occurred. The induction period of the ER-SiO_2/PVDF/SFT-coated samples in the fouling solution A was approximately 12 h, and the induction period in the fouling solution B was about 6 h. Based on the surface free energy similarity principle [68,69], $CaCO_3$ could nucleate at any location with low surface energy and a long induction period. The longer the induction period, the better the anti-fouling efficiency of the coating [70,71].

(3) Anti-fouling efficiency

As shown in Fig. 8 (c), various coatings displayed different anti-fouling effects. In fouling solution A, the anti-fouling efficiency of ER-SiO_2/PVDF/SFT coating reached 1.71 times more effective against fouling than the ER coatings. Similarly in fouling solution B, compared with pure aluminium sheets, the anti-fouling efficiency of ER-SiO_2/PVDF/SFT coating was 1.83 times more fouling efficient than the ER coating, which was 25 % more fouling efficient. The superhydrophobic coating achieved an anti-fouling efficiency of over 70 % in both fouling solutions, which is superior to that of previous studies [15,72]. This outstanding performance can be mechanistically explained by the effective air entrapment within the hierarchical micro-nano structure (observed in Fig. S2), which established a stable Cassie-Baxter state that minimized solid-liquid contact and thus foulant adhesion.

3.4. *Environmental and sustainability benefits*

Coatings could yield both performance and long-term operational benefits by surface functionalization [73], and cross-domain material innovations can open new application pathways [35]. This work applied advanced surface engineering to ZLD systems, supporting circular economy transitions in high-impact industrial sectors. The application of superhydrophobic coatings offers multiple benefits for industrial wastewater treatment and heat exchanger efficiency. By preventing fouling accumulation, the coating minimises corrosion and surface degradation, significantly extending the operational lifespan of industrial equipment and reducing the need for frequent replacements and associated material waste. It also diminishes the need for harsh chemical cleaning agents, thereby lowering toxic effluent discharge and environmental impact. The key advantage lies in its energy-saving potential. As the coating prevents fouling-induced heat transfer losses, it optimises thermal performance and reduces the energy consumption of thermal evaporation processes. This contributes to lower emissions and overall operational cost savings. The superhydrophobic coating supports circular economy principles by all the multifunctional benefits.

From a policy and regulatory perspective, this technology aligns with UN Sustainable Development Goals (SDG) 6 (Clean Water and Sanitation) and SDG 12 (Responsible Consumption and Production) by mitigating industrial water contamination and promoting resource-efficient wastewater management. It also supports ZLD initiatives, which are increasingly adopted by industries worldwide to minimise environmental impact. Table 3 breaks down the circular economy indicators related to this research.

4. Conclusion

To address the persistent fouling challenges in metal heat exchangers, an innovative superhydrophobic coating, ER-SiO_2/PVDF/SFT, was successfully developed. By optimising the PVDF ratio and refining curing conditions, the coating significantly enhanced the substrate's WCA from 137.0 ± 1.5° to 154.3 ± 0.5°. Compared to other advanced antifouling methods, this short two-step fabrication proved to be industrially viable, cost-effective, and scalable, making it a practical solution for high-salinity wastewater treatment. Additionally, the coating exhibited strong adhesion to the substrate, ensuring long-term stability under operational conditions.

The superhydrophobic ER-SiO_2/PVDF/SFT coating demonstrated exceptional antifouling and self-cleaning performance, effectively minimizing fouling accumulation. The results showed a >70 % reduction in fouling deposits in high-salt environments, with easily removable aragonite crystals and sand deposits. Even after seven days of exposure,

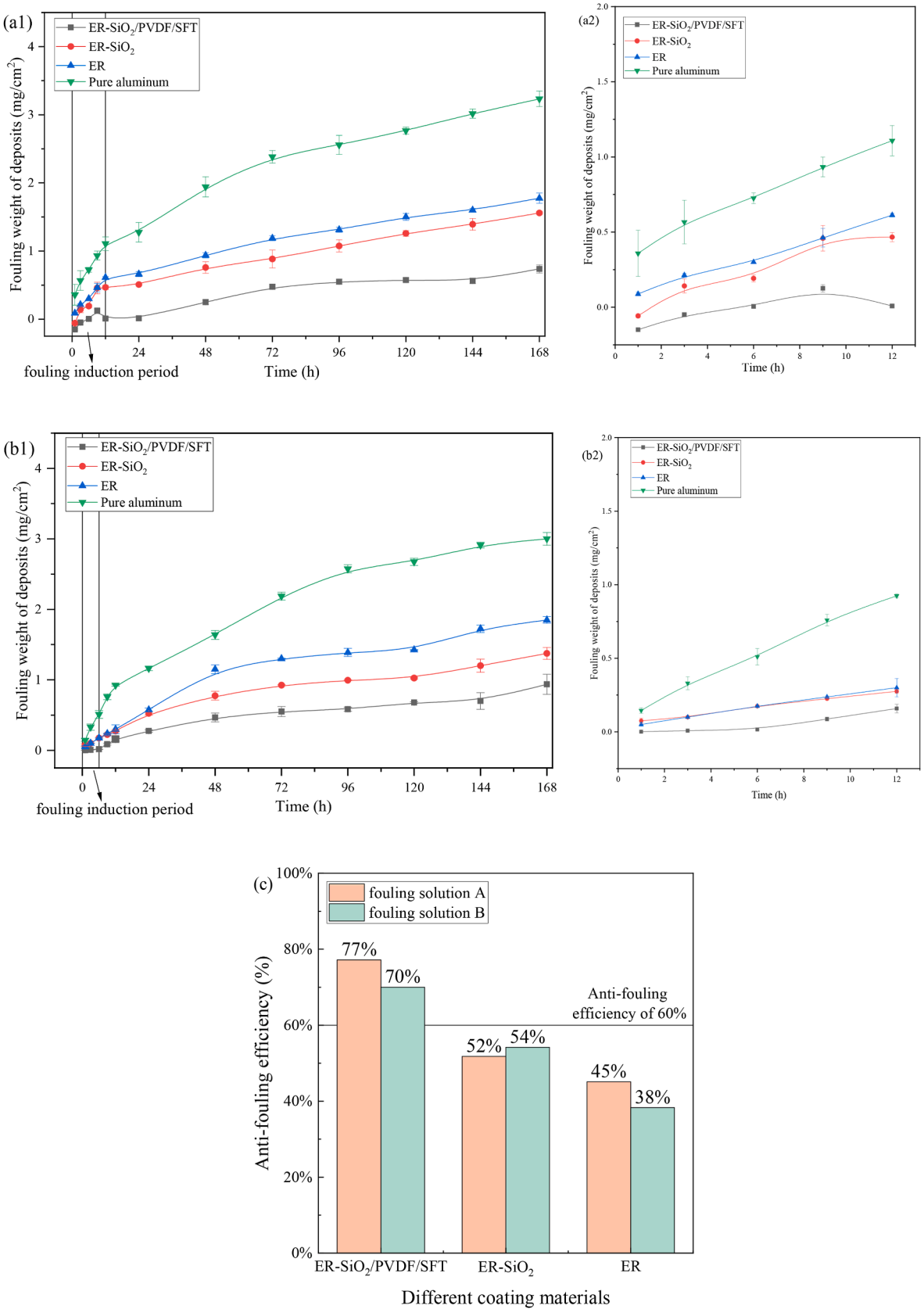

Fig. 8. Analysis of fouling variations for different substrates in fouling solution A and B.

Table 3
Circular economy indicators.

Circular Economy Aspect	Details and Indicators	Approach and Contributions
Design for Sustainability & Durability	Product design to minimise environmental impact and enhance product longevity	The coating's durability extends its lifecycle and reduces the need for frequent replacements. Compared to traditional coatings that degrade quickly, it offers **enhanced fouling resistance** and **long-term performance**, contributing to **closed-loop circularity**.
Manufacturing Process & Waste Minimisation	Processes to reduce resource consumption, energy use, waste generation, and the possibility for repurposing by-products	The two-step synthesis method is energy-efficient and minimises waste, making it more sustainable than traditional multi-step processes. By recycling unused raw materials and repurposing by-products, the approach supports **closed-loop production** and **waste minimisation**
Performance in Use & Economic Impact	Reducing the need for additional chemicals or maintenance and long-term economic sustainability	The superhydrophobic coating minimises fouling, reducing the need for chemical treatments and maintenance, which lowers operational costs. Its extended operational lifespan reduces the need for replacements, making it **cost-effective** and **economically sustainable** for industries.
End-of-Life Management & Recycling Potential	Ensuring recyclability, refurbishment, or repurposing of the coating at the end of its lifecycle	Recycling pathways for fluorosilicon-based coatings are complex but possible, allowing for material repurposing. This development reduces landfill waste and supports **sustainable material recovery**, positioning the coating as a more environmentally friendly option than conventional coatings with limited recycling potential.

the coating retained a high WCA of 145°, highlighting its durability and sustainability.

These findings confirm that the modified superhydrophobic coating provides an environmentally sustainable approach to mitigating fouling, leveraging its low surface energy and weak adhesion properties to prevent deposit buildup. Furthermore, its simple, re-applicable synthesis process aligns with circular economy principles, enabling waste reduction, prolonged equipment lifespan, and improved resource efficiency in industrial water treatment systems. This study underscores the potential for the widespread adoption of sustainable superhydrophobic coatings, supporting resource conservation, industrial water reuse, and energy-efficient wastewater treatment. However, further investigation into the coating's long-term mechanical stability under extreme thermal and conditions will help optimise its durability for large-scale industrial applications.

CRediT authorship contribution statement

Zhigen Wu: Writing – review & editing, Supervision, Methodology, Investigation, Funding acquisition, Conceptualization. **Zihan Yan:** Writing – original draft, Methodology, Investigation, Data curation. **Chenzhen Ji:** Methodology, Conceptualization. **Dan Zhou:** Writing – review & editing, Data curation. **Mohammad Harris:** Writing – review & editing. **Hongwei Wu:** Writing – review & editing.

Declaration of competing interest

The authors declare that they have no known competing financial interests or personal relationships that could have appeared to influence the work reported in this paper.

Acknowledgements

This work was supported by the National Natural Science Foundation of China (52370149), Shandong Excellent Yong Scientists Fund Program (Overseas), China (Grant No. 2023 HWYO-080), and Science and technology innovation project of Hunan Province (2022RC4020).

Appendix A. Supplementary data

Supplementary data to this article can be found online at https://doi.org/10.1016/j.eesus.2025.100055.

References

[1] Wang B, Li H, Jiang Y, Kong X, Xue J, Qiao Y, Liu B, Cheng D, Gao Y, Jiang Q. Solid-liquid phase equilibrium relationship of high salt wastewater of coal chemical industry and mechanism of crystallization and scaling process. J Environ Chem Eng 2023;11:110631.
[2] Gaozhong F, Jie H, Xin J, Weile M, Rui Y, Jinsong G, Fang F, Jixiang Y. Microalgae biofilm photobioreactor and its combined process for long-term stable treatment of high-saline wastewater achieved high pollutant removal efficiency. J Environ Chem Eng 2023;11:111473.
[3] Wen H, Xiong K, Yang H, Zhang P, Wang X. Dynamic mechanism of the microbiota of high-salinity organic wastewater with salt-tolerant yeast and its application. J Environ Chem Eng 2022;10:107377.
[4] Zhang W, Wu M, Yu D, Wang D. Preparation and properties of methyltrichlorosilane grafted modified ceramic membranes for membrane distillation. J Environ Chem Eng 2025;13:115405.
[5] Nabajit D, Susmita D. Multistage interfacial thermal desalination system with metallic evaporators. Desalination 2023;556:116576.
[6] Hasan RA, Abdulqader MA, Alias AB, Hussein NA, Ahmed OK, Keighobadi J, Saleh AM, Hamad ZK, Saleh NM, Mahmood MK. Advancements and performance of evaporative cooling technologies: applications, benefits, and future prospects. KHWARIZMIA 2025;2025:30–41.
[7] Shi J, Huang W, Han H, Xu C. Review on treatment technology of salt wastewater in coal chemical industry of China. Desalination 2020;493:114640.
[8] Panagopoulos A, Haralambous KJ. Minimal Liquid Discharge (MLD) and Zero Liquid Discharge (ZLD) strategies for wastewater management and resource recovery – analysis, challenges and prospects. J Environ Chem Eng 2020;8:104418.
[9] Reinar L, A.S. M., M.I. M.. Dynamic simulation of once-through multistage flash (MSF-OT) desalination process: effect of seawater temperature on the fouling mechanism in the heat exchangers. Comput Chem Eng 2021;155:107515.
[10] Mahmood A. Enhancement of the performance of a solar still using a vibrator. Babylonian J Mech Eng 2023;2023:63–70.
[11] Darand J, Jafarian A. Long-term simulation of crystallization fouling in a forced circulation crystallizer. Int J Heat Mass Tran 2024;231:125845.
[12] Xing H, Jin H, Liu X, Li R, Wang M, Xiang H, Wang C. Effect of NH4Cl fouling on heat transfer process of heat exchange tube under forced convection condition. Int J Heat Mass Tran 2023;217:124826.
[13] Zaza A, Bennouna EG, Iranzo A, Hammami YE, Pino FJ. Optimizing sustainability in hybrid cooling towers: investigating fouling resistance, water quality correlations, modeling, and cleaning strategies for thermal power plants. J Clean Prod 2024;462:142706.
[14] Awais M, Bhuiyan AA. Recent advancements in impedance of fouling resistance and particulate depositions in heat exchangers. Int J Heat Mass Tran 2019;141:580–603.
[15] He J, Wang K, Zhang X, Wu P, Liu C, Jiang W. Efficient antiscaling technology based on superhydrophobicity coupled ultrasonic technology. Ind Eng Chem Res 2022;61:5272–84.
[16] Kukulka DJ, Devgun M. An evaluation of heat transfer surface materials used in fouling applications. Heat Transf Eng 2005;27:42–6.
[17] Förster M, Bohnet M. Modification of molecular interactions at the interface crystal/heat transfer surface to minimize heat exchanger fouling. Int J Therm Sci 2000;39:697–708.
[18] Zhu X, Liang H, Tang X, Bai L, Zhang X, Gan Z, Cheng X, Luo X, Xu D, Li G. Supramolecular-Based regenerable coating layer of a thin-film composite nanofiltration membrane for simultaneously enhanced desalination and antifouling properties. ACS Appl Mater Interfaces 2019;11:21137–49.
[19] Elshaarawy RFM, Mustafa FHA, Sofy AR, Hmed AA, Janiak C. A new synthetic antifouling coatings integrated novel aminothiazole-functionalized ionic liquids

motifs with enhanced antibacterial performance. J Environ Chem Eng 2019;7:102800.
[20] Zhu M, Qian H, Fan W, Wang C, Yuan R, Gao Q, Wang H. Surface lurking and interfacial ion release strategy for fabricating a superhydrophobic coating with scaling inhibition. Pet Sci 2022;19:3068–79.
[21] Ensikat HJ, Ditsche-Kuru P, Neinhuis C, Barthlott W. Superhydrophobicity in perfection: the outstanding properties of the lotus leaf. Beilstein J Nanotechnol 2011;2:152–61.
[22] Cassie ABD, Baxte S. Wettability of porous surfaces. Trans Faraday Soc 1944;40:546–51.
[23] Tian X, Verho T, Ras Robin HA. Moving superhydrophobic surfaces toward real-world applications. Science 2016;352:142–3.
[24] Tzitzilis D, Tsekeridis C, Ntakoumis I, Papadopoulos P. Transition of liquid drops on microstructured hygrophobic surfaces from the impaled wenzel State to the "Fakir" Cassie–Baxter State. Langmuir 2024;40:13422–7.
[25] Wan H, Chen T, Lu Y, Li X, Yu F, Ma Y, Gao Z. A facile one−pot approach to fabricate durable superhydrophobic PU sponge modified with TA−APTES and octadecyltrimethoxysilane for oil−water separation. J Environ Chem Eng 2024;12:114985.
[26] Peng X, Xu T, Ma W, Xie W, Liu H, Huang C, Hou H, Peng X. A new way to construct multifunctional superhydrophobic coating and applications in anti-corrosion, self-cleaning, membrane distillation and water/oil separation. J Environ Chem Eng 2024;12:113782.
[27] Nomeir B, Lakhouil S, Boukheir S, Ait Ali M, Naamane S. Hyper-durable, superhydrophobic/superoleophilic fabrics based on biopolymers and organic and inorganic resins for self-cleaning and efficient water/oil separation applications. New J Chem 2024;48:11757–66.
[28] Zakaria NA, Zaliman SQ, Leo CP, Ahmad AL, Ooi BS, Poh PE. 3D imprinted superhydrophobic polyvinylidene fluoride/carbon black membrane for membrane distillation with electrochemical cleaning evaluation. J Environ Chem Eng 2022;10:107346.
[29] Hui TG, Seng OB, Abbas JZ, Chun LS. Impacts of PVDF polymorphism and surface printing micro-roughness on superhydrophobic membrane to desalinate high saline water. J Environ Chem Eng 2021;9:105418.
[30] Ma W, Yang Z, Asif MB, Zhang Y, Li W, Yang J, Yao S. Scalable-manufactured anticorrosion and wear-resistant superhydrophobic surfaces. ACS Appl Eng Mater 2023;1:519–29.
[31] Pan C, He J, Zhu J, Li S, Li W, Yang W, Li W. Corrosion control by carbon-based nanomaterials: a review. ACS Appl Nano Mater 2024;7:2515–28.
[32] Moawad MN, Hamdona SK, Hegazy GE, Alqazzaz AMF, Madkour FF, Tadros HRZ. Eco-friendly algae-based nanoparticles among other green antifouling paints with in vitro and on-site antimicrobial activity. Algal Res 2025;91:104225.
[33] Zhao Y, Wang J, Fang H, Wang S, Ma X, Cai L, Chen X, Zeng R, Shan Z. Multifunctional coatings on magnesium alloy: integrating superhydrophobicity, anticorrosion, and energy harvesting. Nano Energy 2025;144:111381.
[34] Qian W, Zhou L, Chen A, Liu Y. Designing multilayered C/PDMS/PolyF coatings with durable superhydrophobic and photothermal performances to address icing challenge in industrial environments. Appl Surf Sci 2025;710:163936.
[35] Khan SU, Jamshed W. Self-healing materials in aerospace and automotive engineering: a systematic review of material systems, integration strategies, and application performance. Babylonian J Mech Eng 2025;2025:1–17.
[36] Yang F, Zhang J, Pan J, Liu Y, Yu Y, Wang S. Preparation of superhydrophobic coating on X80 steel and its corrosion resistance in oilfield produced water. Langmuir 2024;40:10250–60.
[37] Nomeir B, Lakhouil S, Naamane S, Ait Ali M, Boukheir S. Durable, transparent and superhydrophobic coating with temperature-controlled dual-scale roughness by self-assembled raspberry nanoparticles. Heliyon 2024;10:34983.
[38] Bouadila S, Shbailat SJ. Solar stills: review. Babylonian J Mech Eng 2023;2023:55–62.
[39] Pan S, Guo R, Björnmalm M, Richardson JJ, Li L, Peng C, Bertleff-Zieschang N, Xu W, Jiang J, Caruso F. Coatings super-repellent to ultralow surface tension liquids. Nat Mater 2018;17:1040–7.
[40] Hu J, Fang Z, Huang Y, Lu J. Fabrication of superhydrophobic surfaces based on fluorosilane and TiO2/SiO2 nanocomposites. Surf Eng 2020;37:1–7.
[41] Niu Y, Abd alla IH, jabur Yk, Jassim SA, mohammed Mk, Sulaiman BH, Alsultan QH, Shawqi OSAd, mohameed Oj, Abed TH, Panessai IYP, Khalaf HAK, Abdulbaqi ASA, Jia ZJ, Wang H, Abdulrahman MM, Nejrs SM. Development of high-effectiveness photocatalytic materials for water purification and environmental remediation. KHWARIZMIA 2023;2023:84–94.
[42] Xue C, Li Y, Zhang P, Ma J, Jia S. Washable and wear-resistant superhydrophobic surfaces with self-cleaning property by chemical etching of fibers and hydrophobization. ACS Appl Mater Interfaces 2014;6:10153–61.
[43] Du X, He J. A self-templated etching route to surface-rough silica nanoparticles for superhydrophobic coatings. ACS Appl Mater Interfaces 2011;3:1269–76.
[44] Sun Y, Liu J, Ming P, Zhao D, Song J. Wire electrochemical etching of superhydrophobic 304 stainless steel surfaces based on high local current density with neutral electrolyte. Appl Surf Sci 2022;571:151269.
[45] Tang J, Zou R, Zhang X, Zhong Y, Li M, Feng Y, Wei X, Wang J. Combination of universal chemical deposition and unique liquid etching for the design of superhydrophobic aramid paper with bioinspired multiscale hierarchical dendritic structure. ACS Appl Mater Interfaces 2022;14:4791–807.
[46] Zhang X, Hu C, Fu X, Zhang S, Li T, Ma B, Ren K. An ultra-thin nickel electrodeposited stainless steel mesh with superhydrophobic property and high mechanical durability for oil-water separation. J Environ Chem Eng 2024;12:111692.
[47] Sun Y, Zhao D, Song J. Electrochemical fabrication of superhydrophobic 304 stainless steel by neutral electrolyte. J Mater Sci 2022;57:20069–81.
[48] Zhu P, Geng J, Zhu L, Wang G, Tang L, Hu H, Zeng Z. Mechanically and boiling water stable superhydrophobic coatings with special composite structures prepared by facile spraying method. J Environ Chem Eng 2025;13:115220.
[49] Pan X, Xinxue L. Fabrication of TiO2/SiO2 superhydrophobic coating for efficient oil/water separation. J Environ Chem Eng 2021;9:105538.
[50] Xue M, Fangyuan J, Fei Q, Zaifang L, Jinhui T, Sixing X, Wei M, Yinhua Z. Polyethylenimine aqueous solution: a low-cost and environmentally friendly formulation to produce low-work-function electrodes for efficient easy-to-fabricate organic solar cells. ACS Appl Mater Interfaces 2014;6:22628–33.
[51] Huang Y, Chen B, Lv Z, Guo F, Huang C. A cost-effective method for robust and anti-corrosive superhydrophobic coatings. SN Appl Sci 2019;1:612.
[52] Teng KH, Kazi SN, Amiri A, Habali AF, Bakar MA, Chew BT, Al-Shamma'a A, Shaw A, Solangi KH, Khan G. Calcium carbonate fouling on double-pipe heat exchanger with different heat exchanging surfaces. Powder Technol 2017;315:216–26.
[53] Pietrelli L, Ferro S, Reverberi AP, Vocciante M. Removal of polyethylene glycols from wastewater: a comparison of different approaches. Chemosphere 2021;273:129725.
[54] Li S, Wang Y, Xu M, Pei H, Guo R, Liu N, Mo Z. Self-cleaning, antifouling PPS@ F-SiO2/TZ coatings with superamphiphobicity and anti-crude-oil adhesion. Prog Org Coating 2025;208:109457.
[55] Wang D, Sun Q, Hokkanen MJ, Zhang C, Lin F, Liu Q, Zhu S, Zhou T, Chang Q, He B, Zhou Q, Chen L, Wang Z, Ras Robin HA, Deng X. Design of robust superhydrophobic surfaces. Nature 2020;582:55–9.
[56] Li X, Gao B, Yue Q, Ma D, Rong H, Zhao P, Teng P. Effect of six kinds of scale inhibitors on calcium carbonate precipitation in high salinity wastewater at high temperatures. J Environ Sci 2015;29:124–30.
[57] Liendo F, Arduino M, Deorsola FA, Bensaid S. Nucleation and growth kinetics of CaCO3 crystals in the presence of foreign monovalent ions. J Cryst Growth 2022;578:126406.
[58] Fu Z, Jin H, Zhang J, Xue T, Wen D. Air film evolution during droplet impact onto a solid surface. Phys Fluids 2021;33:092107.
[59] Djoko KT, Cahyo KA, Nita A, Hasrinah H, Salsabilla CDR, Daffa FM, Febio D. Developing a robust photocatalytic and antifouling performance of PVDF membrane using spinel NiFe2O4/GO photocatalyst for efficient industrial dye wastewater treatment. J Environ Chem Eng 2023;11:109449.
[60] Wu S, Zhao S, Zhai Z, Huang Y, Liu S, Yang H, Zhao Y. Robust halloysite nanotubes modified PVDF membranes with improved wetting resistance for hypersaline wastewater treatment via membrane distillation. J Environ Chem Eng 2024;12:114872.
[61] Wang B, Ji J, Li K. Crystal nuclei templated nanostructured membranes prepared by solvent crystallization and polymer migration. Nat Commun 2016;7:12804.
[62] Shunsuke S, Akira N, Naoya Y, Munetoshi S, Ayako H, Yoshikazu K, Kiyoshi O. Hydrophobicity and freezing of a water droplet on fluoroalkylsilane coatings with different roughnesses. Langmuir 2007;23:8674–7.
[63] Zeng Q, Kang L, Fan J, Song L, Wan S, Liao B, Guo X. Durable superhydrophobic silica/epoxy resin coating for the enhanced corrosion protection of steel substrates in high salt and H2S environments. Colloids Surf A Physicochem Eng Asp 2022;654:130137.
[64] Zhao Y, Wang J, Hu M, Niu Y, Liang N. Fabrication of cement-based superhydrophobic coatings with enhanced self-cleaning property, chemical stability, and UV-radiation resistance. J Build Eng 2024;91:109606.
[65] Nomeir B, Lakhouil S, Boukheir S, Ait Ali M, Naamane S. Recent progress on transparent and self-cleaning surfaces by superhydrophobic coatings deposition to optimize the cleaning process of solar panels. Sol Energy Mater Sol Cell 2023;257:112347.
[66] Hao X, Yang Y, Dong S, Zheng H, Wang R. Robust superhydrophobic self-cleaning coating prepared by silane modified multi-walled carbon nanotubes: a combined experimental and molecular dynamics study. J Mol Graph Model 2024;132:108831.
[67] Nomeir B, Lakhouil S, Boukheir S, Ali MA, Naamane S. Durable and transparent superhydrophobic coating with temperature-controlled multi-scale roughness for self-cleaning and anti-icing applications. Prog Org Coating 2024;189:108338.
[68] Muñoz J, Barril X, Hernández B, Orozco M, Luque FJ. Hydrophobic similarity between molecules:: a MST-based hydrophobic similarity index. J Comput Chem 2002;23:554–63.
[69] Alfredo C. The measurement of the surface energy of solids using a laboratory drop tower. NPJ microgravity 2017;3:25.
[70] Yan ZH, Zhou D, Zhang QH, Zhu YT, Wu ZG. A critical review on fouling influence factors and antifouling coatings for heat exchangers of high-salt industrial wastewater. Desalination 2023;553:116504.
[71] Varnaseri M, Peyghambarzadeh SM. Induction period in crystallization fouling. In: Varnaseri M, Peyghambarzadeh SM, editors. Scale formation in heat exchangers. Cham: Springer Nature Switzerland; 2024. p. 53–80.
[72] Zhu Y, Li H, Zhu M, Wang H, Li Z. Dynamic and active antiscaling via scale inhibitor pre-stored superhydrophobic coating. Chem Eng J 2021;403:126467.
[73] Potharaju S, Jaaz ZA. Development and characterization of antimicrobial nanocoatings for titanium dental implants to prevent peri-implantitis and improve osseointegration. Shifaa 2023;2023:10–8.